Research Article | Vol. 14, No. 8 / 1 Aug 2023 / Biomedical Optics Express 3988
Biomedical Optics EXPRESS

Effect of tissue fixation on the optical properties of structural components assessed by non-linear microscopy imaging

M. Andrea Markus,[1] Daniele P. Ferrari,[1] Frauke Alves,[1,2,3] and Fernanda Ramos-Gomes[1,*]

[1] Translational Molecular Imaging Group, Max-Planck Institute for Multidisciplinary Sciences, Hermann-Rein-Str. 3, 37075 Göttingen, Germany
[2] Clinic of Haematology and Medical Oncology, Institute of Interventional and Diagnostic Radiology, University Medical Center Göttingen, Robert-Koch-Str. 40, 37075 Göttingen, Germany
[3] Cluster of Excellence "Multiscale Bioimaging: from Molecular Machines to Networks of Excitable Cells" (MBExC), Robert-Koch-Str. 40, 37075 Göttingen, Germany
[*] ramos@mpinat.mpg.de

Abstract: Fixation methods such as formalin are commonly used for the preservation of tissue with the aim of keeping their structure as close as possible to the native condition. However, fixatives chemically interact with tissue molecules, such as collagen in the extracellular matrix (ECM) or myosin, and may thus modify their structure. Taking advantage of the second- and third-harmonic generation (SHG and THG) emission capabilities of such components, we used nonlinear two-photon microscopy (NL2PM) to evaluate the effect that preservation methods, such as chemical fixatives, have on the nonlinear capabilities of protein components within mouse tissues. Our results show that depending on the preservation technique used, the nonlinear capabilities of collagen, lipid droplets and myosin microarchitecture are strongly affected. Parameters of collagen fibers, such as density and branch points, especially in collagen-sparse regions, e.g., in kidneys, were found to be altered upon formalin fixation. Moreover, cryo-freezing drastically reduced SHG signals from myosin. Our findings provide valuable information to select the best tissue fixation method for visualization and quantification of structural proteins, such as collagen and myosin by advanced NL2PM imaging techniques. This may advance the interpretation of the role these proteins play in disease.

1. Introduction

Tissue preservation is a method widely used in handling biological specimens. The objective is to maintain the chemical composition and micro-architecture of biological specimens by stopping the activity of catabolic enzymes and the destruction of cellular and extracellular components by microorganisms [1]. Almost any method of tissue preservation has an impact on tissue structure, such as shrinkage, swelling and hardening of tissues with color variations in various histochemical stains [2]. Some fixatives add covalent reactive groups that may induce cross-links between proteins, individual protein moieties, within nucleic acids and between nucleic acids and proteins. Some of the best examples of this group of fixatives are formaldehyde and glutaraldehyde [3,4]. These fixation methods are also commonly used for clinical samples, such as biopsies in combination with routine histopathology. Other storage techniques include cryo-freezing, that is commonly used before cryo-sectioning and has the advantage of better preserving DNA and RNA for genomics and transcriptomics [5].

The use of crosslinking agents can change the configuration of proteins or peptides and may render the epitopes undetectable or unreachable by specific antigens. While fresh tissue even visibly appears different under white light when compared to fixed tissues, there is a shortage

#488453 https://doi.org/10.1364/BOE.488453
Journal © 2023 Received 23 Feb 2023; revised 20 Apr 2023; accepted 25 Apr 2023; published 10 Jul 2023

Biomedical Optics EXPRESS

of studies showing how fixation affects their optical properties, such as scattering, absorption coefficients and polarization properties [6]. In particular, the influence of fixation on optical parameters obtained by multiphoton nonlinear microscopy has not been studied systematically.

Nonlinear two- and three-photon microscopy (NL2PM and NL3PM) provides the possibility of imaging intrinsic signals emitted from second and third harmonic generation (SHG and THG), on top of signals emitted in the form of two-photon excited fluorescence (2PEF). Unlike 2PEF, in which two photons are absorbed by the target structure to produce a fluorescent signal as a single photon with some loss of energy, S- and THG do not involve photon absorption and energy decimation. Instead, they are nonlinear coherent scattering processes involving the conversion of two or three excitation photons into a single emission photon with twice or three times the energy, respectively, and thus, half of the excitation wavelength for SHG and the third part for THG [7].

Biological materials with repetitive non-centrosymmetric units, such as fibrillar collagen or myosin within the striated muscle facilitate the emission of SHG [8]. Both these proteins are integral structural tissue components. Collagen is one of the major proteins expressed in the extracellular matrix (ECM). In muscle tissue, it serves as a major component of the endomysium. 28 types of collagen have been identified, the most abundant of which is collagen I, which is found in all connective tissues as well as blood vessels. Collagen IV can be detected in the basal lamina of epithelial cells and serves as part of the filtration system in capillaries and the glomeruli of nephron in the kidney [9]. Myosins are a superfamily of motor proteins, of which Myosin II (also known as conventional myosin) is the myosin type responsible for producing muscle contraction in skeletal and cardiac muscle cells. Both proteins, collagen and myosin, emit SHG signals which can also be distinguished from another by NL2PM when co-expressed in the same tissue [10]. THG on the other hand, is frequently produced at water-lipid and water-protein interfaces, including intra- and extracellular membranes, lipids and microvesicular structures [11]. Besides this, THG allows visualization of elastin in blood vessel walls, erythrocytes and myelin in peripheral nerve fibers [12,13].

Importantly, the expression of both, collagen and myosin, is highly relevant in disease and aging processes. Collagen is frequently overexpressed in solid tumors and therefore a potential prognostic biomarker for cancer [14,15], especially in ECM rich tumors such as pancreatic ductal adenocarcinoma [16,17]. Moreover, this protein is also overexpressed in fibrosis, the principal pathological process underlying the progression of chronic kidney disease. Here, different types of collagen are highly up-regulated, of which PIIINP and collagen type IV have already been analyzed as potential biomarkers [9,18,19].

Myosin as an integral part of both cardiac and skeletal muscle, is for instance disturbed in several neuromuscular pathologies as well as during age-related fibrosis, as demonstrated in hearts of marmosets [10]. Muscle biopsies are useful for the differential diagnosis of immune mediated myopathies, muscular dystrophies, congenital myopathies, and mitochondrial myopathies [20] and myofibers are frequently disturbed in myopathies [21,22]. Histology of endomyocardial biopsy specimens from patients with heart failure is still considered the gold standard for myocardial fibrosis detection [23]. Accurate quantification of collagen and myosin is thus eminent in both preclinical and clinical research, especially when healthy and diseased tissue are to be compared.

Here we provide evidence that diverse fixation methods and cryo-freezing can negatively impact the SHG and THG signals from the structural components collagen and myosin in kidney and heart tissues of the mouse. In particular, the clinically common fixative PFA drastically reduces SHG signals derived from collagen, while cryo-freezing impacts on myosin signals. Our results suggest that fixation per se or fixation methods should be carefully considered when quantitative analysis of such structural components is envisaged.

Biomedical Optics EXPRESS

2. Materials and methods

2.1. Animals and organ harvesting

Organs were harvested from pathogen-free and healthy female BALB/c mice, 6–57 weeks of age that were sacrificed by CO_2 euthanasia. All animals were housed in a controlled environment with a regular 12 h dark:light cycle, at 22°C and were fed laboratory chow and tap water ad libitum.

2.2. Tissue preparation

Freshly explanted organs, i.e., heart, skeletal muscle and kidneys, were briefly washed in phosphate buffered saline (PBS) and then grouped for the following conditions: (i) fresh unfixed (9 animals), (ii) 24 h 4% paraformaldehyde (PFA) fixed (9 animals), (iii) cryo-frozen unfixed (3 animals) and (iv) storage for 2 days at 4°C, followed by 24 h of fixation by 4% PFA to mimic forensic conditions (3 animals). Fixation using methanol, ethanol and acetone was tested for kidneys using one animal each. For sectioning, organs were embedded in 5% agarose and were cut into 50 µm and 100 µm using a vibratome (VT1000 S; Leica Biosystems). The vibratome tissue sections used for NL2PM were mounted using Aqua Polymount mounting medium (Polysciences). Left over 4% PFA fixed tissue was embedded in paraffin for immunohistochemistry staining.

2.3. Multiphoton nonlinear optical microscopy

Label-free SHG, THG and 2PEF imaging were performed on an upright TriM Scope II multiphoton microscope (Miltenyi Biotec, Bielefeld, Germany) equipped with a tunable femtosecond laser with two independently tunable output channels (Cronus 2P, Light Conversion, Vilnius, Lithuania). The first tunable channel (680 - 960 nm) was used for SHG and 2PEF excitation, while the second tunable channel (950 - 1300 nm) was used for THG excitation. The laser operated between 1-50% of its maximal output power (1.2 W). The pulses were synchronous with a repetition rate of 77 MHz each. Images were acquired using a Zeiss W Plan-Apochromat 20x (NA 1.0) water immersion objective. The backscattered emitted light was split by two longpass dichroic mirrors (Semrock) at 560 nm and 495 nm, and collected by photo-multiplier (H6780-01-LV, Hamamatsu, Herrsching am Ammersee, Germany) and GaAsP detectors (H7422-40-LV, Hamamatsu, Herrsching am Ammersee, Germany). A photo-multiplier tube (Hamamatsu) in the transmission position collected the forwardscattered emitted light gathered by a 1.4 NA condenser lens under the stage. SHG, THG and 2PEF signals were collected using the filter settings 405 ± 10 nm and 525 ± 50 nm, respectively (405/10 and 525/50 BrightLine HD filters, Semrock, AHF Analysentechnik Tübingen, Germany). For the overview images, an image size of 477×477 µm with 1024×1024 pixels and a pixel dwell time of 2.19 µs was used. Mosaic images were acquired using 337×328 µm tiles image size with 1024×996 pixels to achieve adequate image resolution for analysis. Laser power was monitored at the laser source to assure stability over time and highly repeatable results. Incident laser power under the objective was 12 mW at 810 nm. Emitted light was collected with an oil immersion condenser in the forward direction, which optimizes the detection of even weak SHG signals. PMT gain and laser power was always the same for imaging before and after fixation, i.e. images of fresh tissue sections were acquired with optimal parameters, then the tissue was fixed and sections of fixed tissue were imaged with exactly the same parameters as the fresh tissue before. In total, 9 high-resolution mosaic images ($x \approx 3$ mm; $y \approx 2.7$ mm) from fixed and fresh groups were used for quantification of collagen patterns using Twombli (FIJI macro). From the other two groups, cryo-frozen and storage for 2 days, three high-resolution mosaic images of similar sizes were used for the quantification of collagen patterns.

Biomedical Optics EXPRESS

2.4. Histology and immunohistochemistry

Paraffin embedded kidney tissue was cut with a microtome to 2 µm sections. For staining, the sections were deparaffinized (60 °C, 30 min) and rehydrated by a descending ethanol series. Picrosirius red (Sigma Aldrich) and Masson's Trichrome Staining (MTS) (Sigma Aldrich) was used to stain collagen according to the manufacturer's instructions. Immunohistochemistry was performed with rabbit-anti-mouse collagen I (Origene, Cat. No R1038) and collagen IV (Progen; Cat. No 10760) antibodies following pre-treatment with target retrieval solution (pH 9, 100 °C, 20 min), H_2O_2 (10 min, RT) and Seablock (20 min, RT). Subsequently, secondary antibody anti-rabbit horseradish peroxidase (Histofine, Nichirei Biosciences, 30 min, RT), and AEC (3-Amino-9-ethylcarbazole) substrate (20 min, RT) was applied. Washing between each step was done with Tris-(2-Amino-2-(hydroxymethyl)-1,3-propandiol) buffer (2x 5 min, RT). Finally, the sections were covered with Immu-Mount mounting medium (Thermo Scientific) and a cover glass for evaluation by light microscopy. Images were acquired with a Nikon Ti2 fluorescence microscope.

2.5. Image processing and statistical analysis

All images, including volumetric 3D microscopy z-stacks, were processed and analyzed with the software Imaris 9.1.2 (Bitplane), Imaris Stitcher, FIJI (an image-processing package based on ImageJ) and Graph Pad Prism 7.05 (Graph Pad Software, Inc.). Image processing (adjustments in brightness, contrast or gain) was performed exactly the same for fresh tissue images as for the corresponding fixed tissue images. Maximum 3D projections of z-stacks are presented. Quantification of collagen area, number of branchpoints and number of endpoints was performed with the FIJI macro TWOMBLI, according to the pipeline described in Wershof et al. (2021) [24]. Endpoints and branchpoints were normalized to total length of fibers. For statistical analysis, the unpaired t-test was used with a P value of 0.05 as the margin for statistical significance.

3. Results

3.1. Fixation significantly decreases SHG signals from collagen fibers in the ECM of mouse kidneys

We assessed the nonlinear microscopy signals in fresh and fixed kidney sections from normal mouse tissue. Several different tissue fixation procedures were used, including 4% PFA, ethanol, methanol, acetone as well as cryo-preservation. Sections were imaged by NL2PM to assess their influence on SHG and THG signals.

SHG back- and forwardscattered signals revealed quantitative differences, mainly in collagen architecture including individual fibers, depending on tissue preservation and type of organ analysed. Figures 1 and 2 show in 50 µm thick kidney vibratome sections a significant reduction of the visible number of individual fibers when compared to fresh unfixed samples.

In particular, after 4% PFA fixation SHG signals from collagen were preserved only in the collagen-rich regions, e.g. around blood vessels, albeit also reduced (Fig. 1, red arrow heads), while SHG signals from collagen-sparse regions were significantly reduced or undetectable (Fig. 1, yellow arrow heads). These collagen-sparse regions demonstrate fine, intricate collagen fibers, which are most probably composed of collagen IV.

Similar to 4% PFA, ethanol fixation led to reduced SHG signals from the collagen sparse regions (Fig. 2, second last row), but they were still detectable after direct cryo-frozen conservation (Fig. 2, 2nd row). Acetone and methanol had the most drastic negative effect on collagen derived SHG signals, showing a reduction even in collagen-rich areas (Fig. 2, 5th and 7th row). Moreover, they led to the highest 2PEF background signals (Fig. 2, 5th and 7th row).

These data were also quantifiable and revealed that fixed kidney tissue show a strongly reduced fiber area in comparison to fresh tissue, depending on the fixative used (Fig. 3(A)).

Biomedical Optics EXPRESS

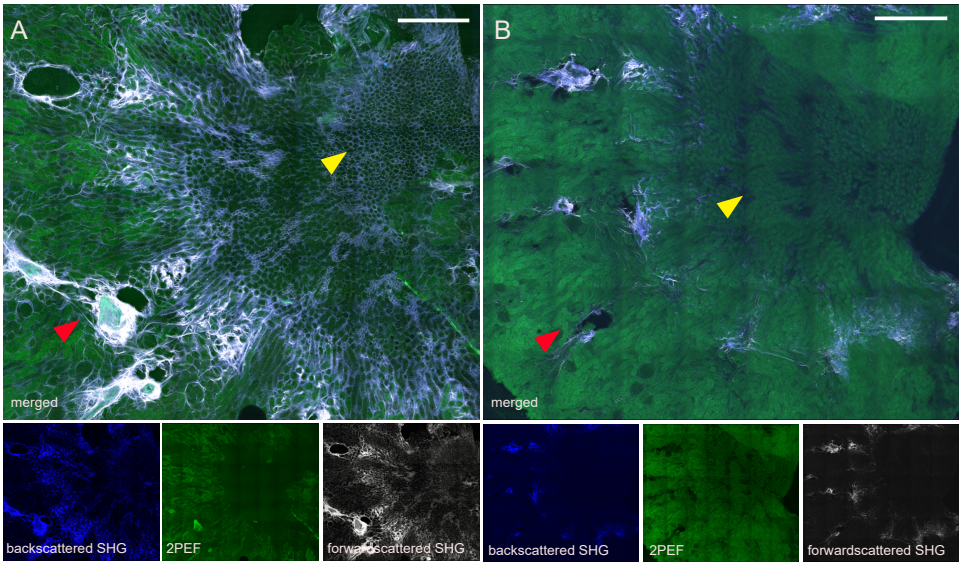

Fig. 1. Fixation reduces SHG signals from collagen of kidney tissue sections. Representative images showing back- and forwardscattered SHG signals from collagen as well as 2PEF in (A) fresh unfixed and (B) 4% PFA fixed 50 µm thick vibratome sections of mouse kidney. The yellow arrow heads mark collagen-sparse regions, while red arrow heads show collagen-rich regions. Upper row shows merged image of bottom row images. Scale bars represent 400 µm.

Especially collagen-sparse regions in the medulla (Fig. 3(A), right graphs) showed a stronger reduction of collagen area in comparison to the cortex (Fig. 3(A), left graphs). Quantification of branchpoints (number of fiber intersections normalized to total length) in the kidney medulla region demonstrates a reduction by 25% in 4% PFA fixed and cryo-frozen tissue (Fig. 3(B)) and an almost complete loss in the 2 days at 4°C stored - 4% PFA fixed kidney tissue (data not shown). This inevitably leads to an increased number of fiber endpoints, showing double as many endpoints after cryo-freezing and ≈1,7 fold more endpoints after 4% PFA (Fig. 3(C)). Based on these results we conclude that 4% PFA fixation and cryo-freezing reduces the fiber pattern complexity of the ECM. In addition to an alteration in fiber metrics, we detected a significant general increase in 2PEF signals in fixed kidney tissues which reached up to 10-fold of those from fresh unfixed tissue (Fig. 3(D) and (E)).

To validate the presence and the types of collagen in the examined fixed kidney tissues we performed a picrosirius red and MTS staining with all types of fixed tissue as well as immunohistochemistry (IHC) on adjacent paraffin sections from 4% PFA fixed tissue with antibodies against collagen I and IV. The picrosirius red and MTS staining confirmed the presence of fine collagen fibers around the tubules of the medulla as well as the stronger collagen expression in the cortex, in particular around blood vessels of the Bowman's capsules (Fig. 4(A) and (B) and Suppl. Fig. 1). Moreover, we found that all kidney tissues expressed collagen I and IV at the expected locations, such as around blood vessels, tubules and in the interstitium (Fig. 4(C)-(D)).

3.2. Cryo-preservation strongly reduces myosin SHG signals in mouse heart tissue sections

In heart tissue, myosin is a strong source of SHG signals. In contrast to collagen, myosin derived signals in mouse 100 µm heart vibratome sections were mostly affected by cryo-freezing (Fig. 5, 1st and 3rd column). The high-resolution visualization of the myosin striation by SHG was no

Biomedical Optics EXPRESS

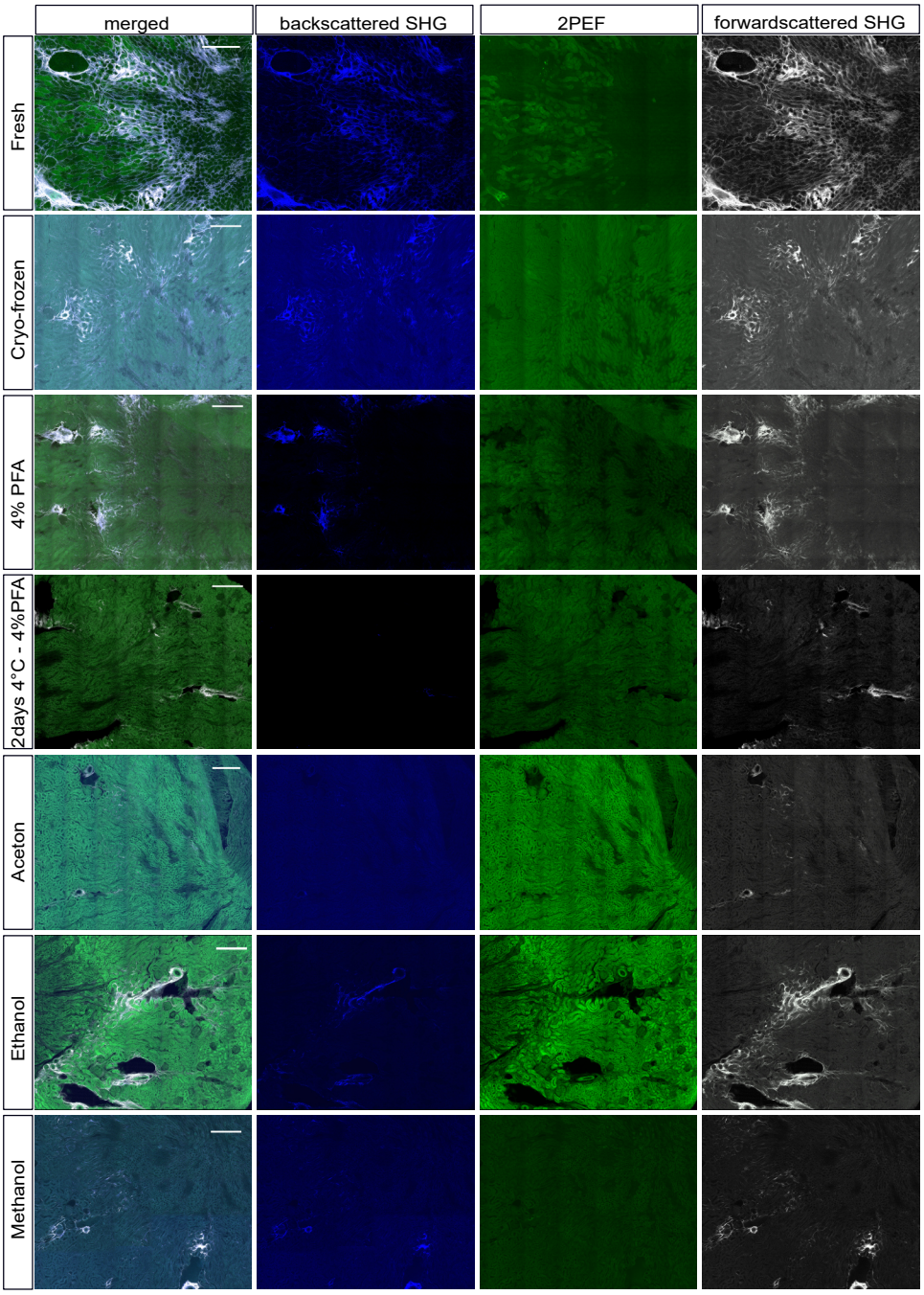

Fig. 2. Fixation reduces SHG signals from collagen in kidney tissue sections. Representative images showing backscattered (2nd column, blue) and forwardscattered (last column, white) SHG signals from collagen as well as 2PEF signals (3rd column, green) in 50 µm thick mouse kidney vibratome sections after the following treatment: (i) fresh unfixed – 1st row, (ii) cryo-frozen – 2nd row, (iii) 4% PFA fixed – 3rd row (iv) 2 days 4°C and 4% PFA fixed – 4th row, (v) acetone fixed – 5th row, (vi) ethanol fixed – 6th row, (vii) methanol fixed – 7th row. Note that all fixations lead to a significant loss of SHG signals, in particular deriving from fine collagen fibers of the kidney medulla. Scale bars represent 300 µm.

Biomedical Optics EXPRESS

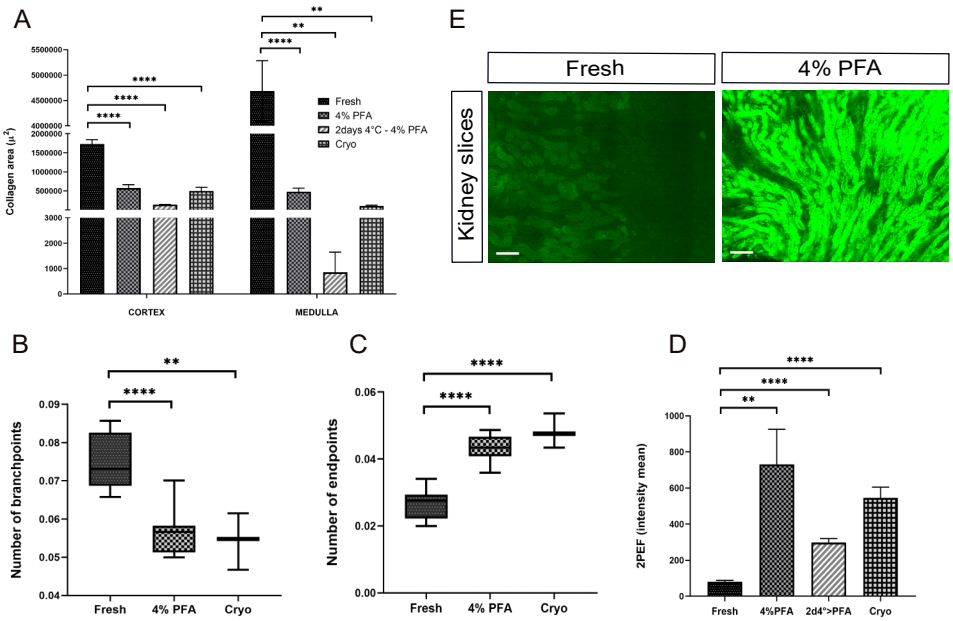

Fig. 3. Quantification of ECM patterns in mouse kidney tissue sections. Quantification of collagen area (A) and 2PEF (D) was performed under the following conditions: (i) fresh unfixed, (ii) 4% PFA fixed, (iii) 2 days 4°C-4%PFA, (iv) cryo-frozen. Quantification of branchpoints (B) and endpoints fiber metrics (C) was performed in fresh unfixed, 4% PFA fixed and cryo-frozen tissues. (E) shows representative images of 2PEF signals from fresh (left) and 4% PFA (right) fixed kidney sections. Scale bar in D represents 100 µm. ** represents $p < 0{,}01$; **** represents $p < 0{,}0001$.

longer possible after cryo-preservation, presumably due to the fragmentation of the proteins (Fig. 5, yellow stars in zoomed images). Cardiac mouse collagen, which is also visible as backscattered SHG in fresh unfixed tissue, was minimally affected by cryo-freezing (Fig. 5, yellow arrow heads in 1st column).

3.3. Fixation modifies THG signals in kidney tissue

We then went on and assessed by NL2PM changes that may occur in THG signals upon fixation. We found that in 100 µm vibratome tissue sections from mouse kidney, signals from lipid droplets and nuclei are clearly reduced after 4% PFA. In fresh unfixed tissue, abundant lipid droplets were visible around the tubules (Fig. 6, 1st row, 3rd column). Moreover, as THG frequently appears at interfaces, tubular nuclei were well visible in fresh tissue (Fig. 6, 1st row, zoomed image). Both these signals were significantly reduced in 4% PFA fixed tissue, in part probably through a fixative-related dehydration of the tissue (Fig. 6, 2nd row, 3rd column and zoomed image). In tissue that we kept at 4°C for 2 days before fixing with 4% PFA to mimic forensic conditions, we found an almost complete loss of THG signals and an increase in 2PEF (Fig. 6, 3nd row, 3rd column and zoomed image), possibly caused by a profound deterioration of the tissue before fixation, which leads to highly autofluorescent dead cells.

In glomeruli, we demonstrate a complete change in the morphological structures that could be visualized by THG. While fresh unfixed glomeruli displayed a strong THG signal from erythrocytes (Fig. 7, 1st row, 3rd column), this signal disappeared after 4% PFA fixation (with

Biomedical Optics EXPRESS

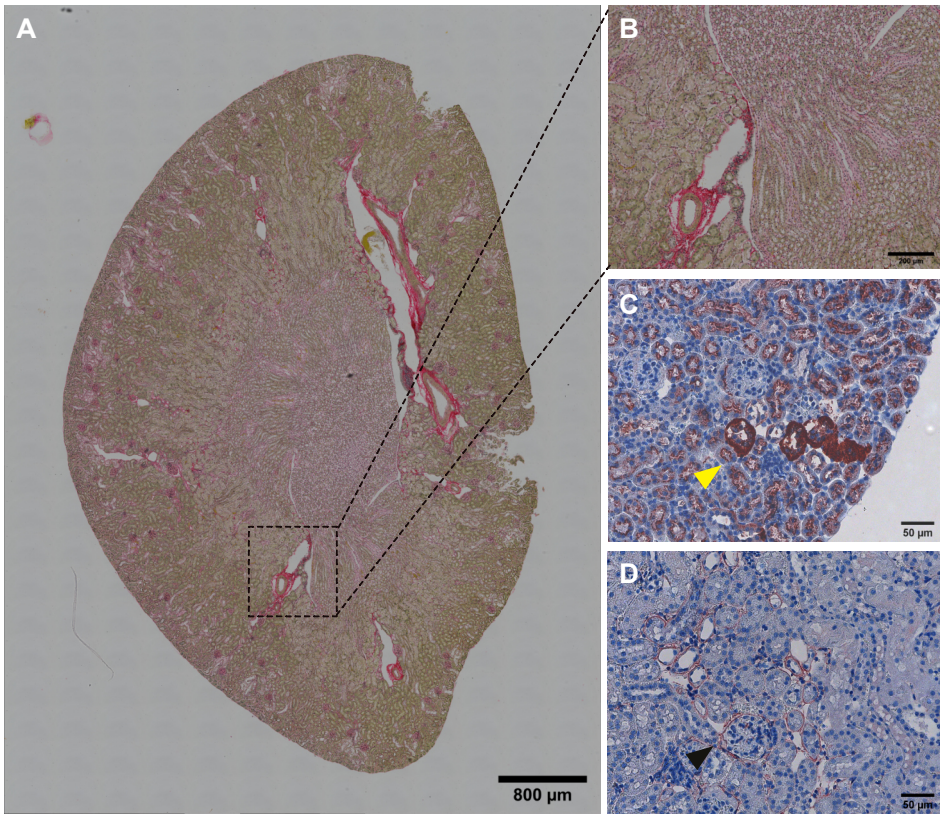

Fig. 4. Histological and IHC validation of the presence of collagen in mouse kidney tissue. Representative images of 2 µm paraffin sections from 4% PFA fixed tissue showing picrosirius staining (A and B = inset of A) as well as IHC staining with anti-collagen I antibody (C) showing expression around tubules (yellow arrow head) and with anti-collagen 4 antibody (D), demonstrating expression in the basal membrane around the tubules and the Bowman's capsules (black arrow head). Scale bars represent 800 µm in A, 200 µm in B and 50 µm in C, D.

and without 2 days storage at 4°C prior to fixation) and instead a changed THG signal appeared that was emitted from the glomerular blood vessels (Fig. 7, 2nd and 3rd row, 3rd column), most probably caused by deteriorated erythrocytes attached to the capillary network of the glomeruli. Here too, we found an increased 2PEF signal after 4% PFA fixation (Fig. 7, 2nd column).

By contrast, the THG signal emitted from elastin present in larger blood vessels did not change after fixation with 4% PFA, showing the preservation of fine elastin fibers in the basal membrane layer of the tunica intima of the blood vessels (Fig. 8, 4th column). As already mentioned before, Fig. 8 (1st column) also impressively shows the complete loss of collagen derived backscattered SHG in kidney tissues that were stored at 4°C for 2 days before fixation of the organ. However, forwardscattered SHG from collagen around the vessels was still visible in these tissues (Fig. 8, 3rd column).

Biomedical Optics EXPRESS

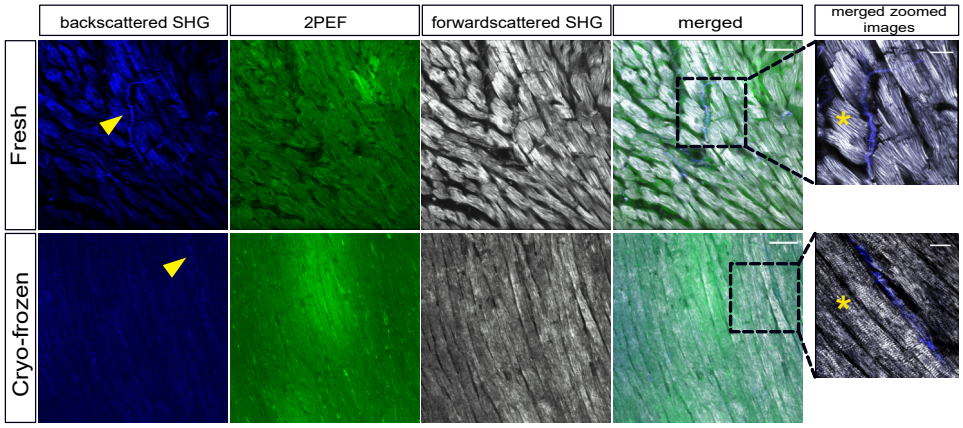

Fig. 5. Cryo-freezing strongly reduces myosin-derived SHG signals in mouse heart tissue sections. Representative images showing backscattered (1st column, blue) and forwardscattered (3rd column, white) SHG signals as well as 2PEF signals (2nd column, green) from collagen and myosin in 100 µm vibratome sections of fresh unfixed (top row) and cryo-frozen sections (bottom row) of mouse hearts. The yellow stars in the zoomed insets of merged images (last column) mark the myosin preserved (top row) versus fragmented (bottom row) regions. The yellow arrowheads mark collagen fibers visible in backscattered SHG. Scale bars represent 200 µm and 20 µm (inset).

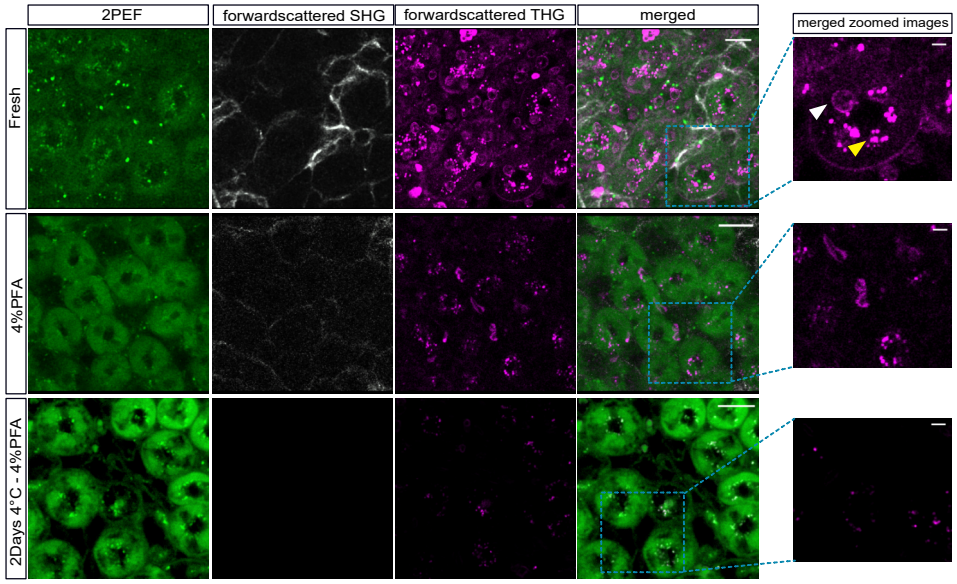

Fig. 6. THG signals from lipid droplets and tubular nuclei are lost after fixation. Representative images showing 2PEF (1st column), SHG signals from collagen (2nd column) and THG signals from lipid droplets and nuclei (3rd column) in vibratome sections of kidney tissue after the following treatment: (i) fresh unfixed – 1st row, (ii) 4% PFA fixed – 2nd row, (iii) 2 days 4°C and 4% PFA fixed – 3rd row. The right panel shows a magnification of the THG signals in the indicated regions. The yellow arrow head marks the lipid droplets; the white arrow head marks a tubular nucleus with THG signal. Scale bars represent 20 µm and 5 µm for zoomed images.

Biomedical Optics EXPRESS

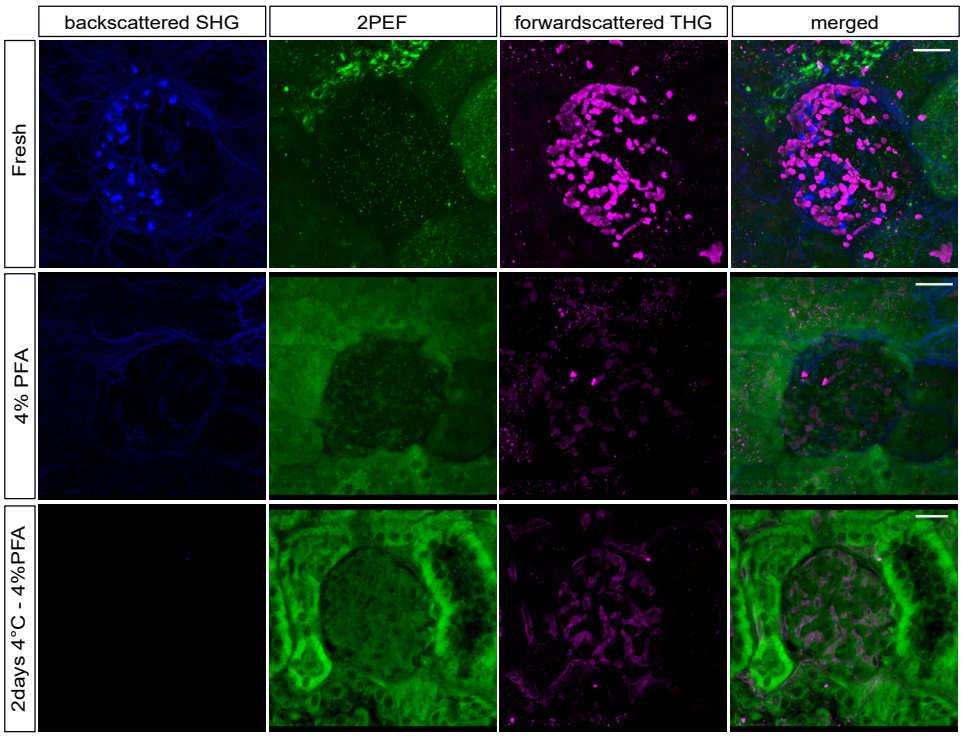

Fig. 7. THG signals from glomerular structures are changed after fixation. Representative images showing SHG signals from collagen (1st column), 2PEF (2nd column) and THG signals from glomeruli (3rd column) in vibratome sections of mouse kidney after the following treatment: (i) fresh unfixed – 1st row, (ii) 4% PFA fixed – 2nd row, (iii) 2 days 4°C and 4% PFA fixed – 3rd row. Scale bars represent 50 µm.

3.4. NL2PM of skeletal muscle benefits from 4% PFA fixation

In contrast to the loss of collagen SHG visualization in kidney tissue and the deterioration of myosin by cryo-preservation, the fixation of skeletal muscle with 4% PFA led to a drastic improvement of the imaging quality. In fresh condition, the muscle loses its contracted form and with this the regular striation pattern of the myofibrils, consisting of the myosin and actin repetitions that make up the sarcomere (Fig. 9(A and B)). Upon 4% PFA fixation, this regularity during contraction is immobilized and yields precise units of the sarcomere building blocks, where myosin could be visualized by its SHG signals and where actin was visible by complementary THG signals (Fig. 9(C and D), inset). As in heart muscle, THG signals could also be generated from lipid depositions located between the muscle fibers (Fig. 9(C)) as well as 2PEF derived from the muscle fibers (Fig. 9(D)).

Biomedical Optics EXPRESS

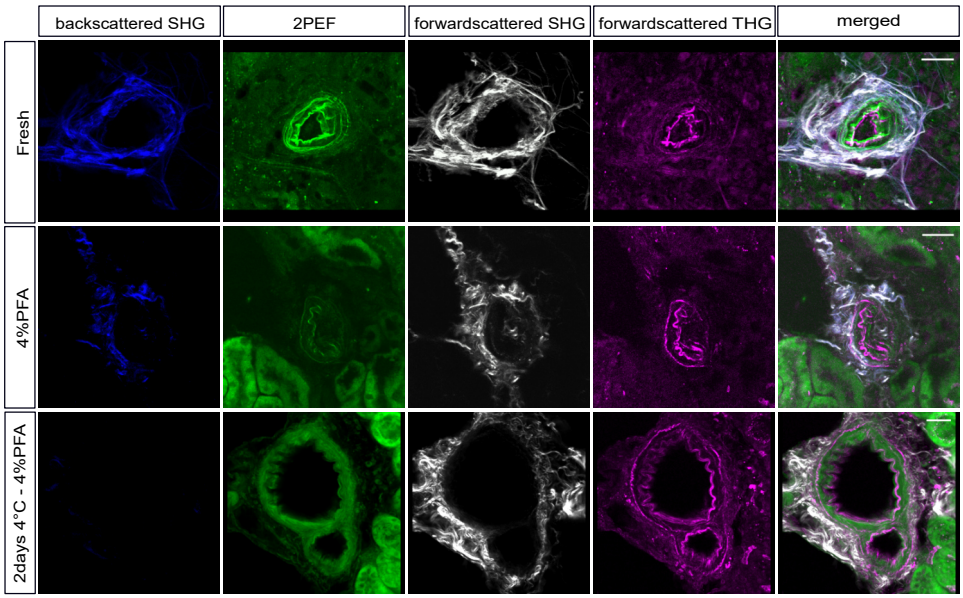

Fig. 8. THG signal from elastin in blood vessels is unchanged after fixation of mouse kidney sections. Representative images showing SHG signals from collagen (1st and 3rd column), 2PEF (2nd column) and THG signals from elastin (4th column) in vibratome sections of mouse kidney after the following treatment: (i) fresh unfixed – 1st row, (ii) 4% PFA fixed – 2nd row, (iii) 2 days 4°C and 4% PFA fixed – 3rd row. Scale bars represent 30 µm.

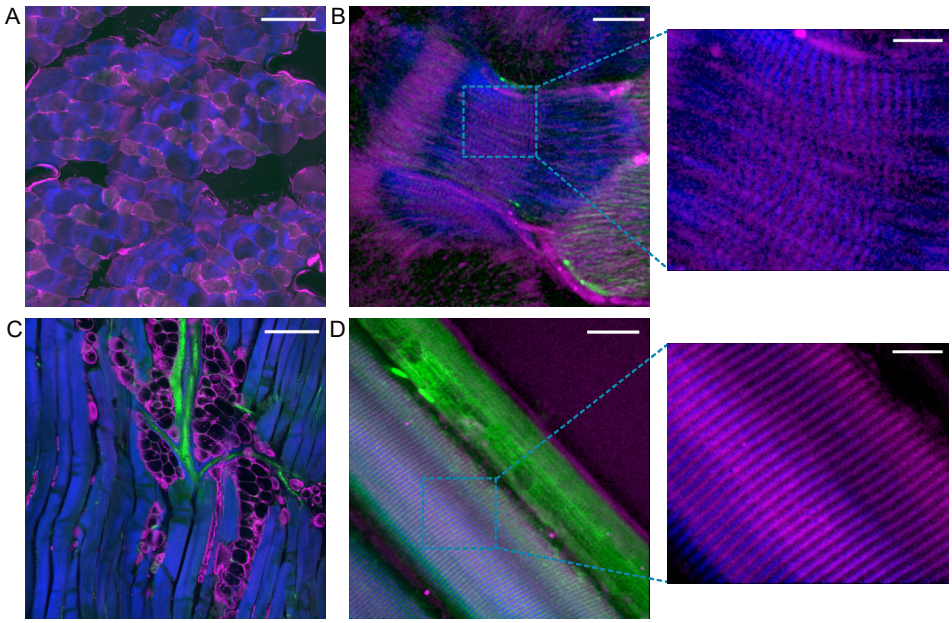

Fig. 9. NL2PM of skeletal muscle benefits from 4% PFA fixation. Representative images showing SHG and THG signals from fresh (A and B) and 4% PFA fixed (C and D) mouse skeletal muscle vibratome sections. SHG signals from myosin (blue), THG signals from actin, lipids and muscle fiber borders (magenta) and 2PEF (green) are visualized. Scale bars represent 200 µm in A and C; 25 µm in B and D and 10 µm in insets.

Biomedical Optics EXPRESS

4. Discussion

Biopsies and other clinical or pre-clinical tissues are frequently fixed for preservation, most commonly with 4% PFA or by cryo-freezing. We show here by NL2PM that these routinely used two tissue preservation methods significantly alter the intrinsic SHG and THG signals from kidney, heart and skeletal muscle tissue. In kidney tissue we found that 4% PFA and ethanol drastically reduced the SHG signals derived from fine interstitial collagen fibers. In cardiac muscle tissue, myosin was significantly impacted by cryo-freezing. Other preservation methods we tested, i.e. methanol and acetone also led to a pronounced loss of SHG signals from collagen. Moreover, THG signals from lipid droplets and nuclei were also reduced in kidney tissue upon 4% PFA fixation, as opposed to elastin derived THG which was not impacted by this fixation method.

The impact fixation or freezing has on SHG and THG signals is associated with changes that these preservation methods have on the optical properties of the proteins that produce these nonlinear signals. Wood and colleagues have shown an increase in both retardance and depolarization post-fixation that can be attributed to a volume increase, resulting in a longer optical pathlength [6]. The increase in retardance and depolarization after fixation may also be due to changes in bulk optical properties. An increase in optical scattering within the tissue after fixation, due to the cross-linking of proteins creating a more highly scattering media, was also confirmed by others using a double-integrating sphere measurement on myocardial tissue [25,26]. Such an increase in optical scattering of the light in the tissue can cause a diminished back- or forwardscattered signal from the tissue to the detector. Fixation can also introduce artefacts and distortions in the tissue that can affect the symmetry of molecules, particularly in three-dimensional structures. One common artefact that can affect symmetry in fixed tissue is shrinkage. This can lead to distortions of the tissue structure and the spatial distribution of molecules within the tissue that are arranged in a specific orientation, such as the non-centrosymmetric structures of collagen [27]. Fixation can also cause chemical modifications to biomolecules such as proteins, nucleic acids, and lipids. These modifications can include crosslinking, oxidation, or other chemical alterations, which can affect the symmetry of molecules in the tissue. For example, crosslinking of proteins can cause changes in the conformation and orientation of the protein structure, which can affect the activity of enzymes or the binding of ligands.

We found a pronounced decrease of SHG signals localized around the glomeruli and tubular region of kidneys, known to express collagen type IV (COL4) [28]. COL4 is a non-fibrillar collagen that forms a network-like structure in basement membranes. It has a more globular structure than fibrillar collagens and is thought to have a low SHG efficiency due to its high symmetry and lack of long-range order. However, previous studies which claimed that COL4 does not emit SHG have either used COL4 in its native form, using collagen gels or used suboptimal conditions for detection of weak SHG signals [29,30]. While we have no direct evidence that the SHG signals detected in these regions of fresh kidneys are originated from COL4, because colocalization with a fluorescent anti-COL4 antibody is not feasible with unfixed tissue, we speculate that in fresh tissue COL4, in association with other proteins present in the basement membrane, is capable of producing SHG signals.

In tissue that was stored for two days at 4°C before fixation, we detected a complete loss of backscattered SHG signal, but could still visualize a signal from forwardscattered SHG, albeit strongly reduced. When collagen fibers undergo changes to their non-centrosymmetric arrangement it will cause a change in SHG polarization dependence. This can lead to differences in forward- and backwardscattered SHG signals, which are differently sensitive to the orientation of the collagen fibers. In the case of the two days stored tissue, the deterioration of the proteins most likely caused a change in the collagen fiber orientation and thus affecting the polarization, which could not be detected anymore in the direction opposite to the incident beam.

Biomedical Optics EXPRESS

While SHG and THG signals are not routinely assessed in clinical pathology, these processes have repeatedly been shown to provide important information on the expression and morphology of structural proteins such as collagen and myosin. The influence of fixation and preservation methods on collagen and myosin quantities or morphology is essential for the assessment of disease degree, classification of subtypes of disease as well as the identification of subtle differences in pathologies with similar symptoms. For instance, in oncology, tumors are frequently characterized by collagen-rich ECM, which plays a role in metastasis and is a prognostic factor for disease outcome. Importantly, the connection of tumor-associated collagen signatures with prognosis and therapy has repeatedly been demonstrated by SHG assessment using NL2PM [31–33]. Furthermore, it was also shown that this imaging methodology was able to reveal changes in breast tumor collagen induced by neoadjuvant chemotherapy [34] and that the ultrastructure of collagen measured by polarimetric SHG microscopy showed differences in certain breast tumor types [35]. Other cancer types have also been studied by SHG and THG imaging, such as brain and skin [36,37]. More recently, Minamikawa et al. were able to detect ultra-early-stage liver fibrosis by SHG microscopy [38]. Gavgiotaki et al. demonstrated that the combination of THG imaging with FTIR spectroscopy was able to distinguish malignant cell grade in human breast tissue biopsies [39]. These examples vividly make it evident that a drastic change in SHG and THG signals by fixation would result in a loss of information particularly about collagen signatures and may prevent a precise diagnosis, disease classification or monitoring the efficacy of therapeutic strategies. As a consequence, patients may not be allocated to the best available therapy.

Similar to the imaging of collagen in cancer and fibrosis, myosin-derived SHG can provide new information as well as diagnostic support in neuromuscular as well as cardiac diseases. As early as 2008, Plotnikov et al. showed that SHG imaging was able to provide measures of muscle contractile integrity that correlated strongly with the decline in skeletal muscle function in three different neuromuscular mouse models and human biopsies [40]. In cardiac muscle, SHG imaging was able to reveal micro-level distortion of myofibrils in a model of cardiac remodeling by pressure overload [41]. Combined, these data also suggest that SHG and THG microscopy have highly translatable value for clinical use. Together with our results, which suggest that SHG imaging of fresh tissue provides a significantly more accurate quantitative outcome of SHG emitting proteins such as collagen and myosin, one could envisage NL2PM for a more rapid, label-free clinical assessment of tissues where these proteins play a significant role. The fast SHG and THG evaluation of the ECM in a tumor biopsy or of the myofibril fibers in a muscle biopsy from a child with suspected muscular dystrophy by means of NL2PM in a clinical setting are most fitting examples here. It was already shown that even minimally invasive SHG based endomicroscopy is feasible for the observation of sarcomere lengths and contractile dynamics in muscular diseases such as amyotrophic lateral sclerosis or muscular dystrophy [42,43]. Most importantly, the decision if and how to fix the tissue before SHG and THG detection strongly depends on the tissue type and the protein to be evaluated. Thus, in the case of tumor biopsies, the tissue should be used fresh and immediately after recovery, as all commonly used fixatives have a severe impact on SHG signals from the ECM compound collagen. In the case of heart muscle, cryo-freezing should be avoided completely, as it affects the detection of myosin. While we did not evaluate cryo-frozen skeletal muscle, we expect that this preservation method has an equally strong negative effect on myosin as on heart muscle. Last but not least, fixation can have a positive effect on the SHG visualization of skeletal muscle and should therefore be the preferred conservation method for this kind of tissue.

In summary our results suggest, that routine collection and pathological assessment of tissues in the clinic should be reconsidered by integrating the quantification of SHG and THG signals and by choosing the optimal preservation/fixation method in dependence of the tissue and the structures of interest before further microscopic analysis.

Biomedical Optics EXPRESS

Funding. H2020 LEIT Information and Communication Technologies (101016457); Horizon 2020 Framework Programme (101034427); H2020 Marie Skłodowska-Curie Actions (861190).

Acknowledgments. We thank Regine Kruse, Bärbel Heidrich and Bettina Jeep for excellent technical assistance. We further thank Dr. Miso Mitkovski and Heiko Röhse from the Microscopy Facility of the MPI for Multidisciplinary Sciences, City Campus for technical assistance.

Disclosures. The authors declare no conflicts of interest.

Data availability. Data underlying the results presented in this paper are not publicly available at this time but may be obtained from the authors upon reasonable request.

Supplemental document. See Supplement 1 for supporting content.

References

1. W. E. Grizzle, J. L. Fredenburgh, and R. B. Myers, "4 - Fixation of Tissues," in *Theory and Practice of Histological Techniques (Sixth Edition)*, J. D. Bancroft and M. Gamble, eds. (Churchill Livingstone, 2008), pp. 53–74.
2. T. J. O'Leary and J. T. Mason, "A molecular mechanism of formalin fixation and antigen retrieval," Am J. Clin. Pathol. **122**(1), 154–155 (2004).
3. J. A. Kiernan, "Formaldehyde, formalin, paraformaldehyde and glutaraldehyde: what they are and what they do," Microsc. Today **8**(1), 8–13 (2000).
4. W. J. Howat and B. A. Wilson, "Tissue fixation and the effect of molecular fixatives on downstream staining procedures," Methods **70**(1), 12–19 (2014).
5. M. Shabihkhani, G. M. Lucey, B. Wei, S. Mareninov, J. J. Lou, H. V. Vinters, E. J. Singer, T. F. Cloughesy, and W. H. Yong, "The procurement, storage, and quality assurance of frozen blood and tissue biospecimens in pathology, biorepository, and biobank settings," Clin. Biochem. **47**(4-5), 258–266 (2014).
6. M. F. G. Wood, N. Vurgun, M. A. Wallenburg, and I. A. Vitkin, "Effects of formalin fixation on tissue optical polarization properties," Phys. Med. Biol. **56**(8), N115–N122 (2011).
7. V. Parodi, E. Jacchetti, R. Osellame, G. Cerullo, D. Polli, and M. T. Raimondi, "Nonlinear Optical Microscopy: From Fundamentals to Applications in Live Bioimaging," Front. Bioeng. Biotechnol. **8**, 585363 (2020).
8. P. Friedl, K. Wolf, U. H. von Andrian, and G. Harms, "Biological second and third harmonic generation microscopy," Curr Protoc. Cell Biol. **34**, Unit 4.15 (2007).
9. J. H. Miner, "Type IV collagen and diabetic kidney disease," Nat. Rev. Nephrol. **16**(1), 3–4 (2020).
10. A. Khan, A. Khan, F. Ramos-Gomes, A. Markus, M. Mietsch, M. Mietsch, R. Hinkel, R. Hinkel, R. Hinkel, F. Alves, F. Alves, F. Alves, and F. Alves, "Label-free imaging of age-related cardiac structural changes in non-human primates using multiphoton nonlinear microscopy," Biomed. Opt. Express **12**(11), 7009–7023 (2021).
11. B. Weigelin, G.-J. Bakker, and P. Friedl, "Third harmonic generation microscopy of cells and tissue organization," J. Cell Sci. **129**(2), 245–255 (2016).
12. L. M. G. van Huizen, N. V. Kuzmin, E. Barbé, S. van der Velde, E. A. Te Velde, and M. L. Groot, "Second and third harmonic generation microscopy visualizes key structural components in fresh unprocessed healthy human breast tissue," J. Biophotonics **12**(6), e201800297 (2019).
13. M. Rehberg, F. Krombach, U. Pohl, and S. Dietzel, "Label-free 3D visualization of cellular and tissue structures in intact muscle with second and third harmonic generation microscopy," PLoS One **6**(11), e28237 (2011).
14. L. Necula, L. Matei, D. Dragu, I. Pitica, A. Neagu, C. Bleotu, C. C. Diaconu, and M. Chivu-Economescu, "Collagen family as promising biomarkers and therapeutic targets in cancer," Int. J. Mol. Sci. **23**(20), 12415 (2022).
15. E. Henke, R. Nandigama, and S. Ergün, "Extracellular matrix in the tumor microenvironment and its impact on cancer therapy," Front. Mol. Biosci. **6**, 1 (2020).
16. C. Tian, Y. Huang, K. R. Clauser, S. Rickelt, A. N. Lau, S. A. Carr, M. G. Vander Heiden, and R. O. Hynes, "Suppression of pancreatic ductal adenocarcinoma growth and metastasis by fibrillar collagens produced selectively by tumor cells," Nat. Commun. **12**(1), 2328 (2021).
17. V. M. Perez, J. F. Kearney, and J. J. Yeh, "The PDAC extracellular matrix: a review of the ECM protein composition, tumor cell interaction, and therapeutic strategies," Front. Oncol. **11**, 1 (2021).
18. K. Tilbury, J. Hocker, B. L. Wen, N. Sandbo, V. Singh, and P. J. Campagnola, "Second harmonic generation microscopy analysis of extracellular matrix changes in human idiopathic pulmonary fibrosis," J. Biomed. Opt. **19**(8), 086014 (2014).
19. F. Genovese, A. A. Manresa, D. J. Leeming, M. A. Karsdal, and P. Boor, "The extracellular matrix in the kidney: a source of novel non-invasive biomarkers of kidney fibrosis?" Fibrog. Tissue Repair **7**(1), 4 (2014).
20. A. Cotta, E. Carvalho, A. L. da-Cunha-Júnior, J. Valicek, M. M. Navarro, S. B. Junior, E. B. da Silveira, M. I. Lima, B. A. Cordeiro, A. F. Cauhi, M. M. Menezes, S. V. Nunes, A. P. Vargas, R. X. Neto, and J. F. Paim, "Muscle biopsy essential diagnostic advice for pathologists," Surg. Exp. Pathol. **4**(1), 3 (2021).
21. L. Mercier, J. Böhm, N. Fekonja, G. Allio, Y. Lutz, M. Koch, J. G. Goetz, and J. Laporte, "In vivo imaging of skeletal muscle in mice highlights muscle defects in a model of myotubular myopathy," IntraVital **5**(1), e1168553 (2016).
22. O. Friedrich, M. Both, C. Weber, S. Schürmann, M. D. H. Teichmann, F. von Wegner, R. H. A. Fink, M. Vogel, J. S. Chamberlain, and C. Garbe, "Microarchitecture is severely compromised but motor protein function is preserved in dystrophic mdx skeletal muscle," Biophys. J. **98**(4), 606–616 (2010).

Biomedical Optics EXPRESS

23. T. Liu, D. Song, J. Dong, P. Zhu, J. Liu, W. Liu, X. Ma, L. Zhao, and S. Ling, "Current understanding of the pathophysiology of myocardial fibrosis and its quantitative assessment in heart failure," Front. Physiol. **8**, 1 (2017).
24. E. Wershof, D. Park, D. J. Barry, R. P. Jenkins, A. Rullan, A. Wilkins, K. Schlegelmilch, I. Roxanis, K. I. Anderson, P. A. Bates, and E. Sahai, "A FIJI macro for quantifying pattern in extracellular matrix," Life Sci. Alliance **4**(3), e202000880 (2021).
25. P.-L. Hsiung, P. R. Nambiar, and J. G. Fujimoto, "Effect of tissue preservation on imaging using ultrahigh resolution optical coherence tomography," J. Biomed. Opt. **10**(6), 064033 (2005).
26. J. W. Pickering, S. A. Prahl, N. van Wieringen, J. F. Beek, H. J. Sterenborg, and M. J. van Gemert, "Double-integrating-sphere system for measuring the optical properties of tissue," Appl. Opt. **32**(4), 399–410 (1993).
27. M. J. Turunen, H. Khayyeri, M. Guizar-Sicairos, and H. Isaksson, "Effects of tissue fixation and dehydration on tendon collagen nanostructure," J. Struct. Biol. **199**(3), 209–215 (2017).
28. A. Boutaud, D.-B. Borza, O. Bondar, S. Gunwar, K.-O. Netzer, N. Singh, Y. Ninomiya, Y. Sado, M. E. Noelken, and B. G. Hudson, "Type IV Collagen of the Glomerular Basement Membrane: Evidence that the chain specificity of network assembly is encoded by the noncollagenous NC1 domains*," J. Biol. Chem. **275**(39), 30716–30724 (2000).
29. A.-M. Pena, T. Boulesteix, T. Dartigalongue, and M.-C. Schanne-Klein, "Chiroptical effects in the second harmonic signal of collagens I and IV," J. Am. Chem. Soc. **127**(29), 10314–10322 (2005).
30. S. Ranjit, A. Dvornikov, M. Stakic, S.-H. Hong, M. Levi, R. M. Evans, and E. Gratton, "Imaging fibrosis and separating collagens using second harmonic generation and phasor approach to fluorescence lifetime imaging," Sci. Rep. **5**(1), 13378 (2015).
31. D. Chen, H. Chen, L. Chi, M. Fu, G. Wang, Z. Wu, S. Xu, C. Sun, X. Xu, L. Lin, J. Cheng, W. Jiang, X. Dong, J. Lu, J. Zheng, G. Chen, G. Li, S. Zhuo, and J. Yan, "Association of tumor-associated collagen signature with prognosis and adjuvant chemotherapy benefits in patients with gastric cancer," JAMA Netw. Open **4**(11), e2136388 (2021).
32. R. A. Natal, J. Vassallo, G. R. Paiva, V. B. Pelegati, G. O. Barbosa, G. R. Mendonça, C. Bondarik, S. F. Derchain, H. F. Carvalho, C. S. Lima, C. L. Cesar, and L. O. Sarian, "Collagen analysis by second-harmonic generation microscopy predicts outcome of luminal breast cancer," Tumour Biol. **40**(4), 1010428318770953 (2018).
33. R. de Andrade Natal, J. Adur, C. L. Cesar, and J. Vassallo, "Tumor extracellular matrix: lessons from the second-harmonic generation microscopy," Surg. Exp. Pathol. **4**(1), 7 (2021).
34. D. E. Desa, M. Bhanote, R. L. Hill, J. B. Majeski, B. Buscaglia, M. D'Aguiar, R. L. Strawderman, D. G. Hicks, B. M. Turner, and E. B. Brown, "Second-harmonic generation directionality is associated with neoadjuvant chemotherapy response in breast cancer core needle biopsies," J. Biomed. Opt. **24**(8), 1–9 (2019).
35. A. Golaraei, L. Kontenis, R. Cisek, D. Tokarz, S. J. Done, B. C. Wilson, and V. Barzda, "Changes of collagen ultrastructure in breast cancer tissue determined by second-harmonic generation double Stokes-Mueller polarimetric microscopy," Biomed. Opt. Express **7**(10), 4054–4068 (2016).
36. N. V. Kuzmin, P. Wesseling, P. C. de W. Hamer, D. P. Noske, G. D. Galgano, H. D. Mansvelder, J. C. Baayen, and M. L. Groot, "Third harmonic generation imaging for fast, label-free pathology of human brain tumors," Biomed. Opt. Express **7**(5), 1889–1904 (2016).
37. R. Cicchi, D. Kapsokalyvas, V. De Giorgi, V. Maio, A. Van Wiechen, D. Massi, T. Lotti, and F. S. Pavone, "Scoring of collagen organization in healthy and diseased human dermis by multiphoton microscopy," J. Biophotonics **3**(1-2), 34–43 (2009).
38. T. Minamikawa, E. Hase, M. Ichimura-Shimizu, Y. Morimoto, A. Suzuki, T. Yasui, S. Nakamura, A. Tsutsui, K. Takaguchi, and K. Tsuneyama, "Assessment of ultra-early-stage liver fibrosis in human non-alcoholic fatty liver disease by second-harmonic generation microscopy," Int. J. Mol. Sci. **23**(6), 3357 (2022).
39. E. Gavgiotaki, G. Filippidis, V. Tsafas, S. Bovasianos, G. Kenanakis, V. Georgoulias, M. Tzardi, S. Agelaki, and I. Athanassakis, "Third Harmonic Generation microscopy distinguishes malignant cell grade in human breast tissue biopsies," Sci. Rep. **10**(1), 11055 (2020).
40. S. V. Plotnikov, A. M. Kenny, S. J. Walsh, B. Zubrowski, C. Joseph, V. L. Scranton, G. A. Kuchel, D. Dauser, M. Xu, C. C. Pilbeam, D. J. Adams, R. P. Dougherty, P. J. Campagnola, and W. A. Mohler, "Measurement of muscle disease by quantitative second-harmonic generation imaging," J. Biomed. Opt. **13**(4), 044018 (2008).
41. J.-D. Nicolas, A. Khan, A. Markus, B. A. Mohamed, K. Toischer, F. Alves, and T. Salditt, "X-ray diffraction and second harmonic imaging reveal new insights into structural alterations caused by pressure-overload in murine hearts," Sci. Rep. **10**(1), 19317 (2020).
42. X. Chen, G. N. Sanchez, M. J. Schnitzer, and S. L. Delp, "Microendoscopy detects altered muscular contractile dynamics in a mouse model of amyotrophic lateral sclerosis," Sci. Rep. **10**(1), 457 (2020).
43. G. N. Sanchez, S. Sinha, H. Liske, X. Chen, V. Nguyen, S. L. Delp, and M. J. Schnitzer, "In vivo imaging of human sarcomere twitch dynamics in individual motor units," Neuron **88**(6), 1109–1120 (2015).